Instantaneous State InSAR: Estimation and Prediction for Near Real-Time Displacement Monitoring

Yuqing Wang, Wietske S. Brouwer, Freek J. van Leijen, *Member, IEEE*, and Ramon F. Hanssen, *Senior Member, IEEE*

***Abstract*—Urban resilience and decision-making rely on continuous monitoring of key safety indicators. The increasing availability of interferometric synthetic aperture radar (InSAR) observations offers a valuable opportunity for near real-time stability monitoring, particularly in the built environment. Traditional InSAR time-series methods use batch processing of all available data at a particular moment in time to estimate static and global displacement parameters, describing the motion of the effective scatterer over the entire evaluated time period. This batch approach limits the agility of the method to adapt to a changing temporal behavior, early anomaly detection, computational efficiency, and the systematic inclusion of newly acquired SAR data. Here, we introduce a new method to capture the complex dynamic behavior of a scatterer by estimating its instantaneous state (IS) instead of using a time-invariant parametric description. The IS estimation and prediction model uses single new SAR acquisitions to provide time updates and measurement updates using a Kalman filter methodology. It imposes smoothness constraints on the displacement signal by modeling the velocity as an exponentially correlated, mean-reverting Ornstein–Uhlenbeck process, thereby enhancing the practicality of the method, and employs the normalized median amplitude dispersion as a proxy for phase quality. The results demonstrate that IS-InSAR matches the estimation quality of batch methods in non-dynamic circumstances while more effectively capturing dynamic behavior. Updating IS with single observations enables near real-time monitoring, and the explicit specification of smoothness parameters facilitates implicit phase unwrapping.**

***Index Terms*—InSAR point scatterers (PSs), instantaneous state (IS), Kalman filter, recursive least squares, smoothness constraints, temporally correlated model.**

I. Introduction

SYNTHETIC aperture radar interferometry (InSAR) enables the precise monitoring of surface and infrastructure stability [1], [2]. This requires a procedure that accommodates a *sequential* approach, i.e., the systematic ingestion after new acquisitions and the subsequent estimation of the relevant parameters. Conventional InSAR methods typically follow a *nonsequential* approach, designed to perform *batch* processing, i.e., using a given and fixed set of SAR data to estimate a predefined set of time-invariant parameters [1], [3], [4], [5]—which is suboptimal for dynamic, real-time monitoring with continuous measurement updates. Batch methods typically have a fixed parameterization [6], assuming that all scatterers follow the same time-invariant model, which is unrealistic in complex urban areas where conditions may change frequently. Moreover, this time-invariant or "static" approach lacks discriminatory power to detect changes in kinematic behavior and is computationally inefficient as new data arrives.

Sequential approaches for InSAR time-series analysis can be represented either by static, global parameters or by kinematic states of the motion of the scatterer. *Parameter-based sequential estimation* assumes that a single set of global time-invariant parameters is used to describe the scatterer's motion over the entire observation period. *State-based sequential estimation* represents the instantaneous kinematic state, e.g., position and velocity, and optionally acceleration [7], [8]. This approach, which explicitly accounts for the dynamic evolution between acquisitions, is the subject of this study.

A. Parameter-Based Sequential Estimation

Sequential estimation can be implemented with time-invariant parameters to describe the scatterer's motion, e.g., the displacement phase or a constant velocity. Recursive estimation, a special case of sequential estimation, can be used to update the parameter estimates from the previous epoch using newly acquired observations through an explicit recursion, without reprocessing the entire time series. Under linear-Gaussian assumptions, i.e., linear state and observation models with additive Gaussian noise, the recursive estimation is equivalent to the Kalman filter [9].

A sequential estimator for phase time series was introduced in 2017 [10], in which the data are divided into small batches and compressed into artificial interferograms. This data reduction enables the artificial interferograms to link earlier batches with newly acquired data, thereby reconstructing the phase time series. An M-estimator was incorporated into the sequential least-squares estimation of the displacement phase to mitigate bias introduced by unwrapping errors present

Received 29 December 2025; revised 23 February 2026; accepted 30 March 2026. Date of publication 6 April 2026; date of current version 17 April 2026. This work was supported in part by "LiveQuay: Live Insights for Bridges and Quay Walls" Project through Dutch Research Council (NWO) (https://www.nwo.nl/en/projects/nwa143120002) under Grant NWA.1431.20.002, in part by SkyGeo (https://www.skygeo.com), and in part by Geodelta (https://www.geodelta.com). *(Corresponding author: Yuqing Wang.)*

The authors are with the Department of Geoscience and Remote Sensing, Delft University of Technology, 2628 CN Delft, The Netherlands (e-mail: y.wang-29@tudelft.nl; w.s.brouwer@tudelft.nl; f.j.vanleijen@tudelft.nl; r.f.hanssen@tudelft.nl).

Digital Object Identifier 10.1109/TGRS.2026.3681072

in both historical and newly added observations [11]. This direct estimation of the displacement phase is commonly employed within the small baseline subset (SBAS) framework, where multiple interferograms between the latest acquisition(s) and earlier ones are generated to estimate the displacement phase of the most recent epoch(s) [12]. This approach can be further combined with the estimation of parameters that describe the scatterer's motion behavior. Sequential adjustment with least-squares Bayesian estimation was applied to the SBAS InSAR procedure to update the deformation parameters, i.e., a constant velocity [13]. This formulation was further developed using modulo-2π ("wrapped") InSAR phases under the premise that the phase differences in the arcs between two epochs of short-baseline interferograms are immune from phase ambiguities [14]. A Kalman filter method was employed for InSAR analysis using a static parameterization, i.e., a linear combination of user-defined functions, such as constant velocity, trigonometric, spline, and Heaviside functions, to solve for the temporal evolution of phase changes with the presumedly "unwrapped" phases generated by SBAS [15]. For point scatterers (PSs), recursive least squares were also introduced for parameter estimation using a constant velocity model as each new observation becomes available [16], [17].

While these approaches employ sequential estimation, their parameterization is static and global. This formulation is optimal when the objective is to derive an efficient model that describes scatterer motion over the entire observation period using a fixed set of parameters, whose numerical values are updated as new acquisitions become available. However, this implies that the parameterization—and therefore the expected behavior of each single scatterer—should be known beforehand. Consequently, the same static and global parameterization can mask changes in scatterer behavior that are not well represented by the chosen model. For these situations, state estimation may be more optimal.

B. State-Based Sequential Estimation

To estimate the kinematic state of InSAR scatterers sequentially, Kalman filter methods have been employed, using a state vector that typically comprises position and constant velocity, together with an acceleration term [18], [19]. Such models assume that the velocity remains constant over time, and its variations are temporally memoryless. In this study, we propose a novel framework for estimating the dynamic instantaneous state (IS) of the scatterer by explicitly modeling the velocity as an exponentially correlated [20], mean-reverting Ornstein–Uhlenbeck process [21], thereby providing a physically constrained stochastic model for the process noise, i.e., an explicit constraint on signal[1] smoothness to enhance robustness and interpretability, hereafter referred to as IS InSAR estimation. The IS parameterization is useful if the objective is not to estimate model parameters that describe how a scatterer moved in the past, but to describe the current (instantaneous) kinematic state of the scatterer, in order to predict a future state, and subsequently update this with new acquisitions as they arrive.

In Section II, we introduce the method for the initialization step of the procedure, followed by the recursive least-squares method for the IS update in Section III. Results for the batch and IS solutions are presented in Section IV, followed by a discussion and conclusions in Sections V and VI, respectively.

II. Initialization for Parameter Estimation

Prior to initiating the recursive IS update procedure, a batch static initialization is performed using an initial set of SAR acquisitions. This initialization is based on individual arcs, which are defined as quasi-vectors connecting a base point (i) to a companion point (j). In the following, we present a generic model for initial parameterization and ambiguity resolution using integer least squares (ILSs), followed by a specific model formulation that explicitly defines the unknown parameters to be estimated, using amplitude data as a proxy quality metric for phase estimation.

A. Generic Model Formulation

For a specific PS[2] j, we denote the single look complex (SLC) phase of the daughter[3] image at epoch t relative to the phase of the mother image (at a reference epoch t_0) as the temporal single-difference observation $\psi_j^{t_0 t}$. Here, $t = 1, \ldots, m_1, m_1 + 1, \ldots, m_2$, where m_1 and m_2 denote the number of observations used for the initialization and for the entire (currently available) observation period,[4] respectively, as elaborated further in Section III-A. The modulo-2π phase for PS j relative to a base point i is referred to as the spatio-temporal double-difference (DD) observation, $\varphi_{ij}^{t_0 t} \in [-\pi, +\pi) \subset \mathbb{R}$, obtained by complex multiplication. As the absolute (nonmodulo-2π) DD phase $\phi \in \mathbb{R}$ is not available, we apply ILS [25] to estimate the integer ambiguities. The functional and stochastic model for an arc can be written as [26]

$$E\left\{\begin{bmatrix}\underline{\varphi}\\ \underline{b}_0\end{bmatrix}\right\} = \begin{bmatrix}\mathbf{F_1} & \mathbf{B}_1\\ \mathbf{F_2} & \mathbf{B}_2\end{bmatrix}\begin{bmatrix}f\\ b\end{bmatrix};\ \text{and}$$
$$D\left\{\begin{bmatrix}\underline{\varphi}\\ \underline{b}_0\end{bmatrix}\right\} = \begin{bmatrix}Q_\varphi & 0\\ 0 & Q_{b_0}\end{bmatrix} \tag{1}$$

where $E\{.\}$ is the expectation operator, $\underline{\varphi} \in [-\pi, +\pi) \subset \mathbb{R}$ is the vector of m_1 DD phase observables, $\underline{b}_0$ is the pseudo observables, and $D\{.\}$ is the dispersion of the observables described by the corresponding variance–covariance matrices (VCMs) Q_φ and Q_{b_0}. f is the vector of the m_1 unknown integer ambiguities ($f \in \mathbb{Z}$), and b is the vector of n unknown parameters of interest, discussed in detail in Section II-B. For each parameter of interest in b, a pseudo observation is added in $\underline{b}_0$. The pseudo observations in $\underline{b}_0$ are required to solve the model rank deficiency. $\mathbf{F_1}$ is an $m_1 \times m_1$ diagonal matrix

[1] In this study, the term "signal" denotes the assumed variability of the underlying true variate, independent of observations and free of noise.

[2] While the method is discussed for PS— [22] using the Delft taxonomy [23]—it is equally applicable for distributed scatterers (DSs) [24].

[3] We refer to "mother and daughters," where the mother image is defined as the reference image.

[4] Note that m_2 changes as new acquisitions arrive.

with -2π on the diagonal, $\mathbf{B}_1$ is an $m_1 \times n$ matrix that transforms the parameters b into the expectation of the absolute DD phase $\underline{\phi}$, $\mathbf{F_2}$ is an $n \times m_1$ zero matrix, and $\mathbf{B}_2$ is an $n \times n$ identity matrix. The float solution $\underline{\hat{c}}$ (i.e., disregarding the integerness of f) and the accompanying VCM $Q_{\hat{c}}$ are obtained using least squares and denoted as follows:

$$\underline{\hat{c}} = \begin{bmatrix} \underline{\hat{f}} \\ \underline{\hat{b}} \end{bmatrix}; \quad Q_{\hat{c}} = \begin{bmatrix} Q_{\hat{f}} & Q_{\hat{f}\hat{b}} \\ Q_{\hat{b}\hat{f}} & Q_{\hat{b}} \end{bmatrix}. \tag{2}$$

Subsequently, the integer ambiguities $\check{f}$ are estimated after optimizing the ambiguity search spaces with the least-squares AMBiguity decorrelation adjustment (LAMBDA) algorithm [25]. The fixed ambiguities are subsequently used to obtain the solution of the unknowns $\underline{\check{b}}$ and the corresponding VCM $Q_{\check{b}}$ by [27]

$$\begin{aligned} \underline{\check{b}} &= \underline{\hat{b}} - Q_{\hat{b}\hat{f}} Q_{\hat{f}}^{-1} \left(\hat{f} - \check{f}\right) \\ Q_{\check{b}} &= Q_{\hat{b}} - Q_{\hat{b}\hat{f}} Q_{\hat{f}}^{-1} Q_{\hat{f}\hat{b}}. \end{aligned} \tag{3}$$

Thus, $\underline{\check{b}}$ and $Q_{\check{b}}$ become the required initial values for starting the recursive update, as elaborated in Section III-A.

B. Static Model Formulation

We consider the modulo-2π DD phase $\underline{\varphi}_{ij}^{t_0 t}$ between PS j and base point i, over the time interval from epoch t_0 to t as follows:

$$\underline{\varphi}_{ij}^{t_0 t} = \underline{\phi}_D + \underline{\phi}_{\Delta H} + \underline{\phi}_{\mu} + \underline{\phi}_{\mathrm{n}} + 2\pi f, \text{ with } f \in \mathbb{Z} \tag{4}$$

where $\underline{\phi}_D$, $\underline{\phi}_{\Delta H}$, $\underline{\phi}_{\mu}$, and $\underline{\phi}_{\mathrm{n}}$ represent the phase components between points i and j over the time interval t_0 to t, attributed to displacement, cross-range distance, thermal expansion, and noise, respectively, and the last term shows the corrective integer ambiguity. The vector of unknown time-invariant parameters b is

$$b = \begin{bmatrix} v & \Delta H & \eta & S \end{bmatrix}^{\top} \tag{5}$$

where v is a constant average velocity,[5] ΔH is the cross-range distance,[6] and η is the arc's thermal expansion factor reacting proportionally to temperature change, following from [2]:

$$\eta = \mu_{\Delta K_t} \cdot L_{\mathrm{LoS}} \tag{6}$$

where $\mu_{\Delta K_t}$ is the linear expansion coefficient, i.e., a material property, and L_{LoS} is the dimension of the object in the line of sight (LoS) direction of the satellite. The last parameter S denotes the phase constant that corresponds to the atmospheric delay and scattering noise difference in the mother image. In the absence of prior knowledge, the pseudo observations, in $\underline{b}_0$, are set to zero and the VCM Q_{b_0} contains a priori chosen variances (σ_v^2, $\sigma_{\Delta H}^2$, σ_{η}^2, and σ_S^2), which provide soft bounds to the range of possible values for the parameters of interest b.

[5]The time-invariant assumption of a constant average velocity is used only in the first approximation for the initialization phase. Its applicability needs to be evaluated per use case.

[6]Note that this is different from the conventional "DEM-error" [28], as it is not an elevation in vertical direction.

In (1), $\mathbf{B}_1$ transforms the time-invariant parameters b into the expectation of the absolute DD phase $\underline{\phi}$, with

$$\mathbf{B}_1 = \begin{bmatrix} -\frac{4\pi}{\lambda} t & -\frac{4\pi}{\lambda} \frac{B_t^{\perp}}{R} & -\frac{4\pi}{\lambda} \Delta K_t & -\frac{4\pi}{\lambda} \end{bmatrix} \tag{7}$$

where $4\pi/\lambda$ converts distance to phase, using the wavelength λ of the radar. The perpendicular baseline $B_t^{\perp}$ is evaluated between the mother and daughter image at epoch t, and the range R is defined from the mother orbit. The ratio $B_t^{\perp}/R$ of the perpendicular baseline and the range is computed for the companion point. The first entry reflects a constant velocity model, used in this initialization stage only. The second entry relates the cross-range distance to the phase observable, while the third entry refers to the relative temperature change $\Delta K_t \equiv \Delta K_{t_0 t}$ between epoch t and the reference epoch t_0. The last entry relates the atmospheric delay and the scattering noise to the phase observable.

We assume no correlation between DD phase observations since: 1) every resolution cell is unique, with its own scattering mechanisms, and the time-variant clutter is uncorrelated between different resolution cells and epochs [29]; 2) the effect of the shared atmosphere of the mother image is accounted for in the functional model and is characterized by the offset S; 3) the displacement is well covered in the functional model, this is the part of the signal of interest and should therefore not be captured in the stochastic model; and 4) atmospheric signal delays are uncorrelated across different epochs. Thus, the VCM of the DD phase observations Q_{φ} can be represented as a diagonal matrix and simplified to

$$Q_{\varphi} = \left(\sigma_{\varphi_i}^2 + \sigma_{\varphi_j}^2\right) \mathbf{I}_{m_1} = \sigma_{\varphi_{ij}}^2 \mathbf{I}_{m_1} \tag{8}$$

where $\mathbf{I}_{m_1}$ is an identity matrix of size equal to the number of observations, and σ_{φ_i}, σ_{φ_j}, and $\sigma_{\varphi_{ij}}$ are the a priori standard deviations of the phase of point i, point j, and arc ij, respectively. These values can be approximated by the normalized median absolute deviation (NMAD) of the amplitude vector a, defined by M_a [30]

$$\mathrm{M}_a = \frac{\mathrm{med}\left(|a - \mathrm{med}\left(a\right)|\right)}{\mathrm{med}\left(a\right)} \tag{9}$$

where med(a) is the median of the amplitude time-series vector a. The derived empirical relation between the NMAD and σ_{φ} is defined conservatively as [30]

$$\sigma_{\varphi} = 1.3\,\mathrm{M}_a + 1.9\,{\mathrm{M}_a}^2 + 11.6\,{\mathrm{M}_a}^3 \tag{10}$$

where "conservatively" implies a confidence level of 97.7% that the actual σ_{φ} is better (i.e., smaller) than the computed value [30]. Herewith, σ_{φ_i} and σ_{φ_j} can be computed, respectively, to estimate $\sigma_{\varphi_{ij}}$ and subsequently the VCM of the DD phase observations, using (8).

III. Recursive Update

After the batch static initialization, the mathematical model for the IS parameterization can be defined, introducing recursive updating using contextual smoothness constraints. We outline how to incorporate new (modulo-2π) observations to the existing time series and demonstrate the processing scheme tailored for InSAR PSs, comparing incremental batch processing, full batch processing, and recursive IS processing.

A. State-Vector Parameterization

In the initialization stage (Section II), we applied the conventional assumption that the parameters are static, global, and identical for all scatterers, which is not realistic for most cases. Especially when time series are longer and/or when the object of study can be considered less rigid, we prefer time-varying parameters to be estimated in recursive form. To allow for changes in the dynamic behavior of a point, we introduce instantaneous velocity as a new parameter. Thus, to model this dynamic behavior, we consider the *IS* of the unknowns, i.e., position and instantaneous velocity, reparametrizing the first elements in the vector of the unknown time-invariant parameters, see (5), to

$$x_t = \begin{bmatrix} P_t & v_t & \Delta H_t & \eta_t \end{bmatrix}^\top \tag{11}$$

where $P_t \equiv P_{t_0 t}$ is the instantaneous LoS position at epoch t, relative to its position at the reference epoch t_0 (hence, it can be regarded as a change in position, i.e., a displacement), while v_t is the instantaneous LoS velocity at epoch t.[7] While including v_t in this vector may seem superfluous at first glance—since P_t already describes the relative position signal and velocity can be considered the first derivative of the position—both parameters are actually nonrelated and estimated independently and *not* as mere derivatives of the position. Thus, the new design matrix will be

$$\mathbf{A_t} = \begin{bmatrix} -\frac{4\pi}{\lambda} & 0 & -\frac{4\pi}{\lambda}\frac{B_t^\perp}{R} & -\frac{4\pi}{\lambda}\Delta K_t \end{bmatrix}. \tag{12}$$

The first entry transforms the position P_t into radians. The second entry is null since the position is captured in P_t, while v_t is not yet relevant in the expectation of $\underline{\phi}_t$. The initial values for IS $\underline{\hat{x}}_0$ and the corresponding VCM $Q_{\hat{x}_0}$—equal to $\underline{\check{b}}$ and $Q_{\check{b}}$, respectively—can be computed with (3). We now rename the estimator $\underline{\hat{x}}_t$ to $\underline{\hat{x}}_{t|t}$, i.e., the estimator at epoch t, given the time-series data up to and including epoch t. The important computational consequence for computing the latest least-squares estimator $\underline{\hat{x}}_{t|t}$ is that there is no need to store the previous observations $[\underline{\phi}_1, \ldots, \underline{\phi}_{t-1}]$. That is, once the initial $\underline{\hat{x}}_t$ is known, the updated estimator $\underline{\hat{x}}_{t|t}$ can be recursively computed from: 1) the previous estimator; $\underline{\hat{x}}_{t-1|t-1}$; 2) its corresponding VCM $Q_{\hat{x}_{t-1|t-1}}$; and 3) the new observation $\underline{\phi}_t$.

The prediction of the IS from the previous epoch $t-1$ to the current epoch t, here referred to as the *state transition*, follows from:

$$\underline{\hat{x}}_{t|t-1} = \Phi_{t,t-1}\, \underline{\hat{x}}_{t-1|t-1} \tag{13}$$

where $\Phi_{t,t-1}$ is an $n \times n$ transition matrix that relates the estimated parameters $\underline{\hat{x}}_{t-1}$ for epoch $t-1$, to the predicted values of these parameters $\underline{\hat{x}}_t$ at epoch t in the future. The exact formulation of the transition matrix will be elaborated as follows; for now, we consider it as given.

Equation (13) requires the assumption that the state transition can be adequately described with a single matrix, $\Phi_{t,t-1}$. Obviously, this will not be realistic for most practical applications. To relax this assumption and "close" the equation, we introduce the *difference vector* $\underline{d}_{t,t-1}$ (denoted as $\underline{d}_t \equiv \underline{d}_{t,t-1}$ for brevity) to explicitly model deviations from the assumed state evolution of $\underline{x}_t$. Within the Kalman filter framework, $\underline{d}_t$ plays the role of *process noise* [9], accounting for unmodeled signal variability, see Fig. 1.

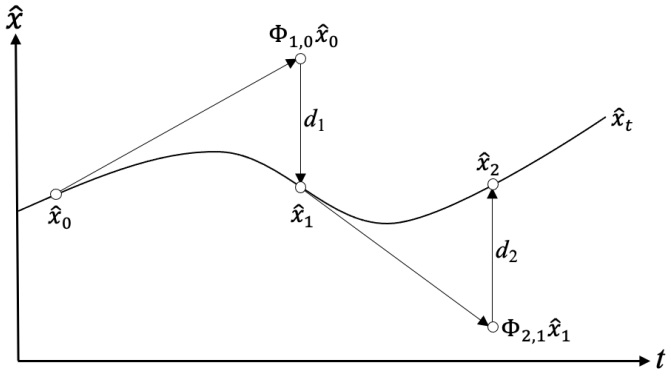

Fig. 1. Schematic of the state transition $\hat{x}_t = \Phi_{t,t-1}\hat{x}_{t-1} + d_t$, where x represents a 4-D hyperspace with the four unknown states of (11). In the time-update equation, the transition matrix $\Phi_{t,t-1}$ predicts the new position in the hyperspace, while difference vector d_t "closes" the difference between the prediction and the true position in the hyperspace x_t.

The difference vector $d_{t,t-1}$ incorporates the changes to the steady-state parameters (e.g., due to an unforeseen velocity change) and is of the same dimension and unit as x_t. This enhances the state transition, see (13), to the *time-update equations*, with the corresponding VCM included [20],

$$\begin{aligned} \underline{\hat{x}}_{t|t-1} &= \Phi_{t,t-1}\, \underline{\hat{x}}_{t-1|t-1} + \underline{d}_t \\ Q_{\hat{x}_{t|t-1}} &= \Phi_{t,t-1}\, Q_{\hat{x}_{t-1|t-1}}\, \Phi_{t,t-1}^\top + Q_{d_t} \end{aligned} \tag{14}$$

where $\underline{\hat{x}}_{t|t-1}$ is the *predicted IS,* given the measurements up to and including $t-1$.

Without any further constraints, it would be impossible to infer or estimate difference vector, and it would be impossible to distinguish measurement errors from actual physical motion. One effective constraint is to impose a level of temporal correlation (smoothness) in the physical behavior of the signal, to be derived from contextual information. Here, we assume an exponentially correlated instantaneous velocity, using an Ornstein–Uhlenbeck process [21], leading subsequently to a temporally "smooth" behavior in position [20], as discussed in Appendix. It is assumed to follow a zero-mean Gaussian distribution and can thus be characterized by the auto-covariance function:

$$C_v(\Delta t) = \sigma_v^2 e^{-\Delta t/\tau} \quad \text{with } \tau > 0 \tag{15}$$

where Δt is the time interval between two epochs. The function is defined by two parameters: 1) the standard deviation of the instantaneous velocity, σ_v; and 2) the decorrelation time of the instantaneous velocity, τ. They describe the velocity behavior of the expected displacement signal and consequently the behavior of the relative position. They are external contextual parameters and should follow from expert elicitation or from empirical experience. They are important as they ultimately define the expected smoothness of the time series, i.e., including the admissible integer phase ambiguities. The standard deviation of the instantaneous velocity σ_v describes

[7] Since our approach is currently tailored toward the monitoring of short arcs, less than 400 m, we can safely disregard the atmospheric noise [1].

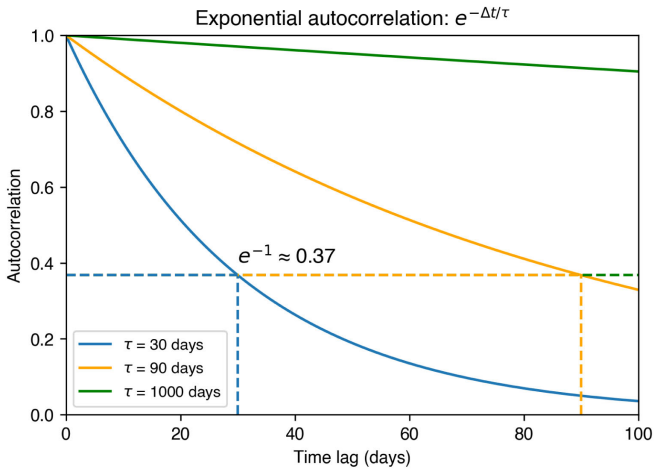

Fig. 2. Exponential autocorrelation of the instantaneous velocity as a function of Δt for decorrelation times (τ) of 30, 90, and 1000 days. Notably, the correlation reaches e^{-1} (≈ 0.37) when $\Delta t = \tau$.

TABLE I
EFFECT OF σ_v AND τ ON THE TREND AND SMOOTHNESS OF THE SIGNAL. THE TERMS "SMALL" AND "LARGE" FOR σ_v AND "SHORT" AND "LONG" FOR τ ARE RELATIVE RATHER THAN ABSOLUTE

	Short τ	Long τ
Small σ_v	Small trend; low smoothness	Medium trend; high smoothness
Large σ_v	Medium trend; low smoothness	Large trend; high smoothness

the magnitude of the steady-state behavior. If the signal is relatively steady, this value will be small (e.g., $\sigma_v = 0.1$ mm/year), indicating a relatively small trend signal. In contrast, in areas with variable subsurface dynamics, the value will be larger (e.g., $\sigma_v = 20$ mm/year), reflecting a relatively large trend signal.

As illustrated in Fig. 2, the exponential autocorrelation is presented as a function of the time lag, Δt, for decorrelation times τ of 30, 90, and 1000 days. The correlation corresponding to a given decorrelation time τ is $e^{-1} \approx 0.37$. The Ornstein–Uhlenbeck assumption for velocity, i.e., (15), suggests that the mean-reverting velocity at a given time is statistically related to its past values and that this dependence decays exponentially with time. A longer decorrelation time results in a slower decay, resulting in a smoother signal. A shorter decorrelation time indicates that the velocity varies more rapidly, which suggests a rougher signal. Thus, different combinations of (σ_v, τ) result in varying overall trends as well as smoothness, see Table I.

For convenience, we provide a simulation tool that allows one to select and adjust σ_v and τ values to generate realizations of the corresponding simulated noise-free signals. This facilitates the selection of appropriate smoothness parameter settings for the expected signal behavior.

The transition matrix $\Phi_{t,t-1}$ of (13) can now be expressed as (see Appendix) [20]

$$\Phi_{t,t-1} = \begin{bmatrix} 1 & \tau\left(1 - e^{-\Delta t/\tau}\right) & 0 & 0 \\ 0 & e^{-\Delta t/\tau} & 0 & 0 \\ 0 & 0 & 1 & 0 \\ 0 & 0 & 0 & 1 \end{bmatrix}. \tag{16}$$

The transition model for exponentially correlated velocity includes $e^{-\Delta t/\tau}$ as an entry, representing the correlation function. When the time step Δt becomes much larger than τ, this value approaches zero, causing the velocity to effectively decorrelate and converge to the expected value—zero. The IS vector, see (11), is augmented with two time-invariant parameters, ΔH and μ. The time invariance results in a null variance for those components of the difference vector. Without prior knowledge, the difference vector d_t is assumed to be zero. Its covariance Q_{d_t} implicitly imposes a temporal smoothness constraint on the state evolution, controlling how rapidly the state can deviate from its predicted value, and is given by [20]

$$Q_{d_t} = \sigma_v^2 \begin{bmatrix} q_{11} & & & \text{sym.} \\ q_{21} & q_{22} & & \\ 0 & 0 & 0 & \\ 0 & 0 & 0 & 0 \end{bmatrix} \tag{17}$$

with (see Appendix for derivation)

$$\begin{aligned} q_{11} &= 2\tau\left[\Delta t - \frac{3\tau}{2} + 2\tau e^{-\Delta t/\tau} - \frac{\tau}{2}e^{-2\Delta t/\tau}\right] \\ q_{21} &= 2\tau\left[-e^{-\Delta t/\tau} + \frac{1}{2}\left(1 + e^{-2\Delta t/\tau}\right)\right] \\ q_{22} &= \left[1 - e^{-2\Delta t/\tau}\right] \end{aligned}$$

where sym. indicates a symmetric matrix and Δt indicates the absolute value of the time difference between epoches t and $t-1$. These matrices are then used in the *time-update equation*, see (14). As a result of the assumption of a constant velocity in the initialization, the initial value for velocity, to initialize the recursive equations, is assumed to be zero with the predefined variance σ_v^2.

Once the prediction $\underline{\hat{x}}_{t|t-1}$ is obtained, see (14), the *updated IS* $\underline{\hat{x}}_{t|t}$ and the corresponding VCM $Q_{\hat{x}_{t|t}}$ can be computed by including the new observation $\underline{\phi}_t$ using the *measurement-update equation* [20]

$$\begin{aligned} \underline{\hat{x}}_{t|t} &= \underline{\hat{x}}_{t|t-1} + Q_{\hat{x}_{t|t}}\mathbf{A_t}^\top Q_{\phi_t}^{-1}\left(\underline{\phi}_t - \mathbf{A_t}\underline{\hat{x}}_{t|t-1}\right) \\ Q_{\hat{x}_{t|t}} &= \left(Q_{\hat{x}_{t|t-1}}^{-1} + \mathbf{A_t}^\top Q_{\phi_t}^{-1}\mathbf{A_t}\right)^{-1}. \end{aligned} \tag{18}$$

Hence, the *updated IS* $\underline{\hat{x}}_{t|t}$ is a weighted sum of the *predicted IS* and the new observation, which can subsequently be used for predicting $\underline{\hat{x}}_{t+1|t}$ via the *time-update equation*, see (14).

The recursive equations would be straightforward when the absolute DD phases, $\underline{\phi}_t$, are known, see (18). Yet, as all interferometric observations are inherently modulo 2π, we make an assumption about the *predicted residual* between the absolute phase observation and its corresponding prediction at

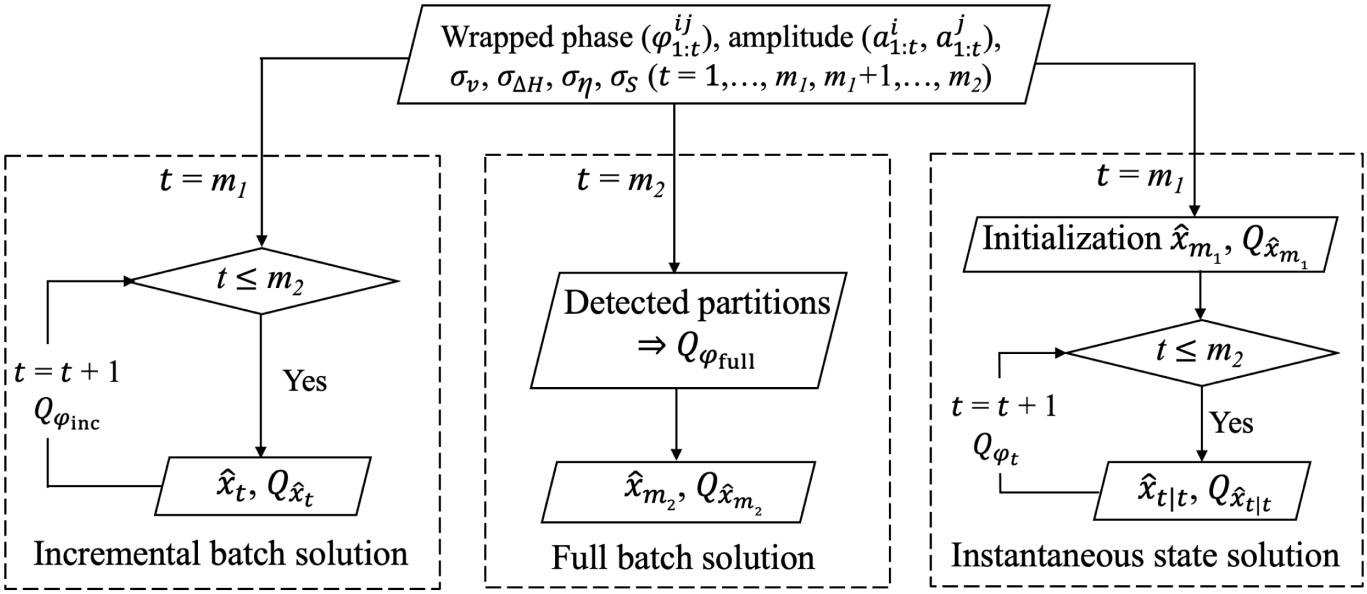

Fig. 3. Flowchart of parameter estimation with three options: the incremental batch solution, the full batch solution, and the proposed IS solution for an individual InSAR arc.

each epoch. Specifically, the *predicted residual* is defined as follows:

$$\Delta\underline{\phi}_t = \underline{\phi}_t - \mathbf{A_t}\underline{\hat{x}}_{t|t-1}. \tag{19}$$

It is assumed that this *predicted residual* lies within half a wave cycle, i.e., a quarter of the radar wavelength, such that

$$|\Delta\phi_t| < \pi \tag{20}$$

known as the *minimum gradient* assumption. While this assumption is heuristic and will obviously not always be correct, observations of good quality will provide good predictions, ensuring that the model follows the motion of the scatterer. The *predicted residual* thus can be written as follows:

$$\Delta\underline{\phi}_t = \mathcal{W}\left\{\underline{\varphi}_t - A_t\underline{\hat{x}}_{t|t-1}\right\} \tag{21}$$

where $\mathcal{W}$ is the modulo 2π ("wrapping") operator [1], in this case transforming $\Delta\phi_t$ to the $[-\pi, \pi)$ interval. Under this condition, the *measurement update* (18) can be written as follows:

$$\begin{aligned}\underline{\hat{x}}_{t|t} &= \underline{\hat{x}}_{t|t-1} + Q_{\hat{x}_{t|t}}\mathbf{A_t}^\top Q^{-1}_{\varphi_t}\mathcal{W}\left\{\underline{\varphi}_t - \mathbf{A_t}\hat{x}_{t|t-1}\right\}\\ Q_{\hat{x}_{t|t}} &= \left(Q^{-1}_{\hat{x}_{t|t-1}} + \mathbf{A_t}^\top Q^{-1}_{\varphi_t}\mathbf{A_t}\right)^{-1}.\end{aligned} \tag{22}$$

This implies that the absolute phase $\underline{\phi}_t$ can be unambiguously resolved with (19) and (21).

B. Processing Scheme

The processing scheme of "IS InSAR" is aimed at InSAR arcs, see Fig. 3.

It starts with a set of SLC data (referred to as "daughters") coregistered to a common reference ("mother") SLC, from which the reference phase and DEM phase are removed to derive the temporal single-difference observations. For a specific arc connecting PS j relative to a base PS i, we perform complex multiplication to obtain the spatio-temporal DD phase observation $\underline{\varphi}_t$.

As discussed in Section II-B, we use the amplitude of each PS to approximate its phase quality σ^2_φ. If the amplitude changes abruptly and significantly, we expect that the corresponding value of σ^2_φ may have changed as well. To account for this, we divide the time series into multiple partitions,[8] each exhibiting its own distinct behavior. Provided that there are sufficient observations within each partition, both the NMAD and consequently the phase quality can be estimated per partition [30]. We select partitions with a duration of at least half a year to account for potential seasonal variations in the amplitude behavior of the scatterers. The observations are then divided into R partitions φ_{p_r} $(r = 1, 2, \ldots, R)$ for the arc ij. We estimate the NMAD for each partition using (9) and approximate σ_φ with (10). The corresponding VCM $\mathbf{Q}_{\varphi_{\text{full}}}$ is then given by the following equation:

$$\mathbf{Q}_{\varphi_{\text{full}}} = \bigoplus_{r=1}^{R}\left(\sigma^2_{\varphi_{p_r}}\mathbf{I}_{p_r}\right) \tag{23}$$

where $\bigoplus$ denotes the direct sum [32] forming a block diagonal matrix, $\sigma^2_{\varphi_{p_r}}$ is the standard deviation of the phase observations in partition p_r, and $\mathbf{I}_{p_r}$ is the identity matrix of size $n_{p_r} \times n_{p_r}$, with n_{p_r} being the number of observations in partition p_r.

To evaluate the IS InSAR method, we also implement both the full batch and the incremental batch processing method. In the batch processing, we apply ILS to resolve the ambiguities and estimate the parameters, see (5), using predefined standard deviations for the parameters (σ_s, σ_v, σ_{Δ_H}, and σ_μ), considering both incremental and full time series. For the *incremental batch* approach, we use the time

[8]This is performed using the pruned exact linear time (PELT) algorithm, which optimizes the segmentation by minimizing a cost function plus a penalty term based on the statistical properties of the time series (e.g., mean or variance) [31].

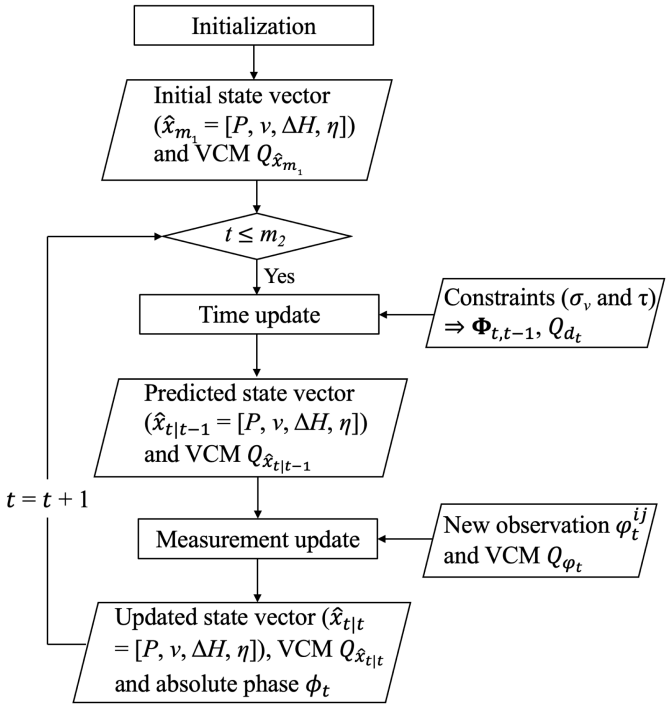

Fig. 4. Flowchart of IS estimation (Fig. 3, right) for an individual InSAR arc.

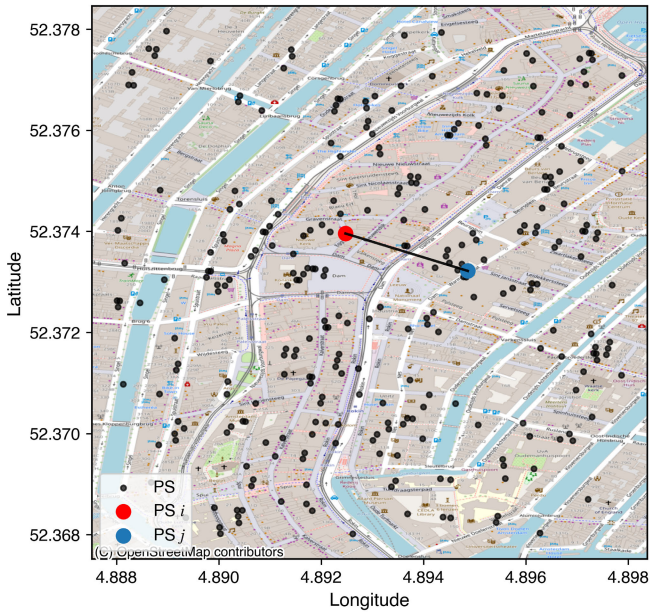

Fig. 5. Map of the AoI in Amsterdam, The Netherlands. The black dots represent the PS used in this study. The red and blue dots indicate the positions of PS i and PS j, respectively, while the black line between them indicates the arc.

series $\varphi_{ij}^{1:t}$, where t is incrementally growing, starting with the initialization length m_1 and then subsequently concatenated with update epochs $[m_1 + 1, m_1 + 2, \ldots, m_2]$ as acquisitions arrive. The corresponding VCM is

$$\mathbf{Q}_{\varphi_{\text{inc}}} = \text{diag}\left(\sigma^2_{\varphi_{m_1}} \mathbf{1}_{m_1},\ \sigma^2_{\varphi_{m_1+1}},\ \sigma^2_{\varphi_{m_1+2}},\ \ldots,\ \sigma^2_{\varphi_t}\right) \tag{24}$$

where diag denotes a diagonal matrix; $\mathbf{1}_{m_1}$ is the m_1-D vector of ones; and $\sigma^2_{\varphi_{m_1}}$ and $\sigma^2_{\varphi_t}$ ($t \in \{m_1 + 1, \ldots, m_2\}$) denote the variances of the phase observations during the initialization and at update epoch t of the incremental time series, respectively. These incremental time series and the corresponding VCM are used to estimate the unknowns $\underline{\hat{x}}_t$, the same as b in (5), and its corresponding VCM $Q_{\hat{x}_t}$ by (3). This is referred to as the *incremental batch solution*. For the full time series, when available, we can estimate a more accurate stochastic model using the VCM $Q_{\varphi_{\text{full}}}$, see (23), for the detected partitions. We then apply ILS again, incorporating partitioned quality estimation to estimate $\underline{\hat{x}}_{m_2}$ and $Q_{\hat{x}_{m_2}}$, where m_2 is the total number of acquisitions available. This is referred to as the *full batch* solution.

In the IS estimation, see Fig. 4, we first apply ILS to the initial 50 epochs to obtain the initial IS estimates. We estimate the *predicted IS* ($\underline{\hat{x}}_{t|t-1}$ and the VCM $Q_{\hat{x}_{t|t-1}}$) for the new epoch using the predefined standard deviation of velocity σ_v and the decorrelation time of velocity τ, and this is the time-update step. As a new observation becomes available, we then use the new modulo-2π phase ($\underline{\varphi}_t$) and the updated VCM, see (9) and (10)

$$Q_{\varphi_t} = \left[\sigma^2_{\varphi_t}\right] \tag{25}$$

to adjust the predicted IS, see (22). This measurement-update step yields the *updated IS* ($\underline{\hat{x}}_{t|t}$ and the VCM $Q_{\hat{x}_{t|t}}$) and the corresponding absolute phase (ϕ_t), see (19) and (21).

IV. Results

We demonstrate IS InSAR to analyze nine years of Sentinel-1 data for a selected area of interest (AoI) in Amsterdam, The Netherlands. The IS estimation approach is compared to: 1) the incremental batch approach; and 2) the full batch approach, choosing one specific arc as an example. Subsequently, we extend this comparison for all selected PS within the AoI and investigate how the estimates change when the parameters of the smoothness constraint vary.

A. Batch and IS Solution

Fig. 5 shows the AoI over the city center of Amsterdam.

Following the approach sketched in Fig. 3, we select PSs—the black dots in Fig. 5—whose NMAD, estimated from the initialization dataset (the first 50 epochs), is smaller than 0.13, i.e., $\sigma_\varphi < 1$ mm for C-band, see (10). The red and blue dots indicate the positions of PS i and PS j, respectively. Fig. 6 shows the amplitude and the corresponding NMAD of PS i (red) and PS j (blue). Fig. 6(a) shows the amplitude (dots) and the corresponding NMAD (solid line) and the detected partitions. The amplitude of PS j indicates anomalous behavior between 2017 and 2018, resulting in a partition with a greater NMAD. In Fig. 6(b), the dashed lines show the constant batch-NMAD estimated using the full amplitude time series. In contrast, the solid lines show the *retrospect* representation of NMAD, estimated from an incrementally expanding amplitude time series. The term retrospect, indicated with (r) in the figure, is used here explicitly to indicate that, at each instant of time after initialization, the value is computed using

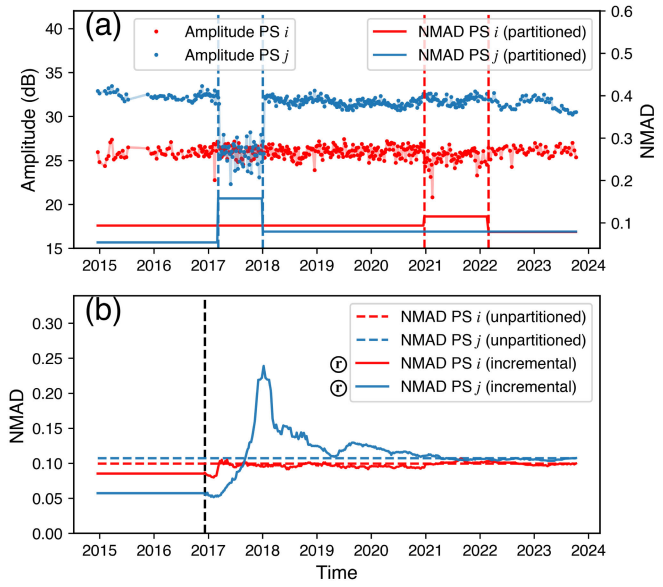

Fig. 6. Amplitude and NMAD of PS i (red) and PS j (blue) of Fig. 5. (a) Left y-axis shows the amplitude of PS i and PS j, and the right and y-axis shows the corresponding NMAD with detected partitions. (b) Dashed lines show the unpartitioned NMAD estimated using the full amplitude time series, and the solid lines show the retrospective NMAD values estimated with the incremental amplitude time series. The circled lowercase r (ⓡ) indicates retrospective values, i.e., quantities depending only on past and present data. This symbol is adopted hereinafter. These solid lines for NMAD are used for the incremental batch solution and the IS InSAR solution.

only the observations available in the present and past, i.e., it follows a causal system [33] that does not depend on future data or the entire time series.[9] These retrospective-NMAD values are thus used for the incremental batch solution and the IS solution. For PS j, the retrospective-NMAD reaches a peak at the end of the detected anomalous partition between 2017 and 2018, after which it gradually retreats to a new asymptote, corresponding with the batch solution.

Fig. 7 shows the solutions of the four elements of the IS vector defined in (11), for the incremental batch, full batch, and IS estimation approaches of the selected arc connecting PS i and PS j.

Fig. 7(a) presents the relative position P_t for the three approaches. The dots in different colors represent the reduced phase, i.e., the DD phase observations after subtracting the components attributed to the estimated cross-range distance and thermal expansion, see (4) and Fig. 7(c) and (d). This shows that minor differences can be observed among the three approaches. The blue and orange dots generally coincide, indicating that the reduced phases derived from the IS solution (orange dots) are consistent with those from the full batch solution (blue dots). This suggests that the proposed minimum gradient assumption, see (20), is reasonable for this example. The batch solution (the blue line) completely misses the 2017–2018 anomaly, as it is tuned to estimate global static parameters. When applied incrementally (the green line) with a growing time series (i.e., the *retrospective* estimate at each epoch is only based on the available data up until that time), the incremental batch solution lags behind the changes in 2017 and 2018, and it takes about two extra years of data acquisitions to converge to the actual values. Clearly, the IS estimation approach (the orange line) fits the observations much better than the two batch approaches and is able to adapt to the changing circumstances more quickly.

Fig. 7(b) shows the instantaneous velocity for the IS solution and the average velocity for the two batch solutions. In the IS solution, the instantaneous velocity is explicitly adopted in the functional model and is constrained with predefined parameters $\sigma_v = 3$ mm/year and $\tau = 150$ days. Note that the instantaneous velocity is not derived through differentiation of the estimated relative positions, but treated as an independent state variable and is estimated separately. This provides a comprehensive state estimation of the dynamic system. Fig. 7(c) and (d) shows the estimates for the cross-range distance (dependent on the elevation of the scatterers) and for the thermal expansion factor, respectively, based on the three approaches. Obviously, the full batch approach (blue) has the advantage of hindsight, i.e., the availability of all observations of the full time series. Thus, the blue lines should not be interpreted sequentially over time, but their final values can be interpreted as near optimal, since they use all available data. In contrast, the results of the incremental batch and IS estimation approaches should be interpreted per epoch, based only on the retrospective information at that time. After initialization, the IS estimation approach (orange) performs better and faster than the incremental batch approach (green) in providing estimates comparable to the full batch solution, converging toward the full batch solution at the final epoch. In general, the IS estimation approach yields solutions of comparable quality to those of the full batch method while effectively capturing the dynamic changes in the time series and operating without access to future data.

B. Geospatial Analysis

As introduced in Fig. 5, 285 PSs with NMAD < 0.13 from the initialization dataset are selected. Among these, the PS with the smallest NMAD, i.e., best expected phase quality, is chosen as the initial reference point.

A total of 284 arcs are then generated between the reference point and the other PSs. In Fig. 8, we compare the geospatial results from the full batch [(a), (d), and (g)] and the IS [(b), (e), and (h)] estimation approaches, where the difference between the two is shown in (c), (f), and (i).

The rows of Fig. 8 show: (a)–(c) the average LoS velocity v, (d)–(f) the cross-range distance ΔH, and (g)–(i) the thermal expansion factor η of these PSs relative to the reference point. Again, the predefined parameters of the IS solution are conservatively set to $\sigma_v = 3$ mm/year and $\tau = 150$ days.

The largely near-zero differences in Fig. 8(c), (f), and (i) show that most of the arcs have comparable results whether in full batch or IS, which demonstrates the compliance of our smoothness-constrained IS estimation method. The means of the differences of v, ΔH, and η are −0.03 mm/year, −0.02 m, and 0.002 mm/K, respectively.

[9]The retrospective nature of the values shown in the figures must be emphasized, since each value is based only on information available up to that time, even though the plots span the full time period. The human eye is nevertheless tempted to interpret given line graphs in their entirety.

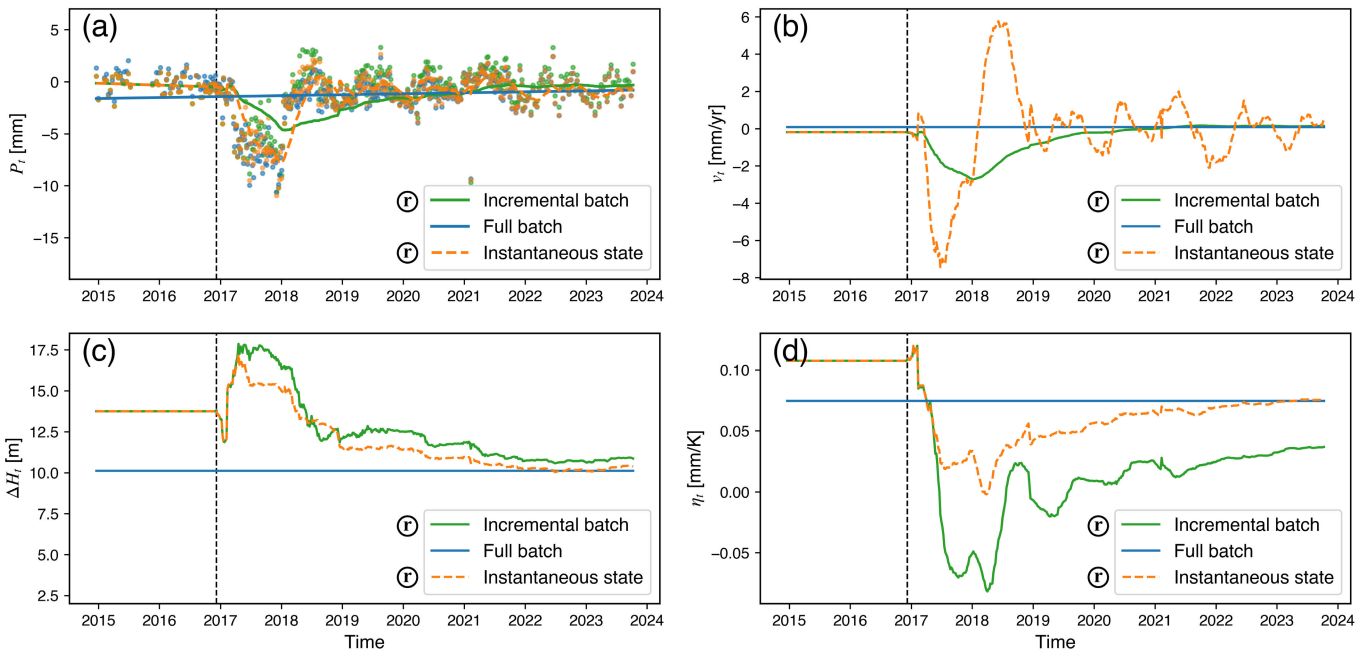

Fig. 7. Four parameters of the incremental batch solution (green), full batch solution (blue), and IS solution (orange dashed) of the arc shown in Fig. 5. (a) Relative position P_t. (b) Instantaneous velocity v_t for the IS solution and the average velocity for the two batch solutions. (c) Cross-range distance ΔH_t. (d) Thermal expansion factor of the arc η_t, see (5) and (11). The black dashed lines indicate the last (50th) epoch of the initialization.

PS1–PS4 in Fig. 8(c), plotted with larger symbol sizes, are four representative examples to illustrate the differences between the two estimation methods. Their corresponding positions (P_t) over time, relative to the reference point, are shown in Fig. 9, where the full batch solution is depicted in blue and the IS solution (i.e., retrospect representation) is displayed in orange.

The displacement signal of PS1 exhibits a noisier episode since mid-2020, alongside fluctuations in the time-series behavior. The IS solution is more likely to adjust effectively to these observations, while the batch solution exhibits more frequent cycle slips after mid-2020, which result in undesirable unwrapping errors. For PS2, the behavior changes around mid-2019. The IS solution adapts to this shift and captures the evolving dynamics, while the batch solution fails to reflect it, as its parameters remain numerically unchanged by definition.

While the difference between the two methods for PS3 is limited, the IS solution is able to capture its dynamic behavior better, particularly the uplift observed in early 2018.

PS4 experienced a displacement change in early 2018. Following this change, the two approaches exhibit distinct unwrapping solutions. The IS solution shifts to a different ambiguity level, while the batch solution yields a result with one ambiguity level lower, which will be further elaborated in Section IV-C.

These examples suggest that while no particular method can claim to be "correct," the IS solution, which lacks the full batch advantage of hindsight, achieves comparable performance while more effectively capturing dynamic behavior. Moreover, as the conventional batch estimation with a fixed parameterization leads to one single solution, alternative solutions that are almost equally feasible remain hidden. In contrast, the IS-InSAR approach makes these alternatives explicit by varying the smoothness constraints, thereby illustrating the sensitivity of InSAR results to modeling choices. We argue that it is more transparent to acknowledge the possibility of multiple plausible solutions (as reflected in the IS formulation) than to focus exclusively on one batch solution.

C. Evaluation of the Smoothness Constraints

Given the distinct ambiguity resolution results produced by the batch and IS solutions for PS4 (Fig. 9), we use this example to demonstrate the influence of the smoothness constraints on the signal.

Fig. 10 shows the instantaneous position (P_t) of PS4 relative to the reference point shown in Fig. 8(c) with different constraints. Fig. 10(a) is the default solution. Increasing σ_v [Fig. 10(a) and (b)] and/or τ [Fig. 10(a) and (c)] introduces more flexibility into the signal, allowing the model to respond more quickly to changes in the dynamic behavior. In addition, Fig. 10(b) and (c) demonstrates that relatively small values of σ_v or τ yield results that more closely align with the conventional linear model, due to the more limited range of permissible variations. In Fig. 10(d), the model more quickly captures the variation around 2018 compared to the solution in Fig. 10(a), thus the smoothness parameters can be tuned to better capture the dynamics in the behavior. It is worth noting that similar results can arise from different combinations of σ_v and τ, as illustrated in Fig. 10(a) and (d), and (b) and (c). Conversely, variations in either σ_v or τ can also lead to distinct outcomes. As a result, ambiguity resolution is inherently controlled by the predefined parameters σ_v and τ, leading to *implicit phase unwrapping* [34]—where the ambiguities are not *explicitly* resolved *before* parameter estimation, but

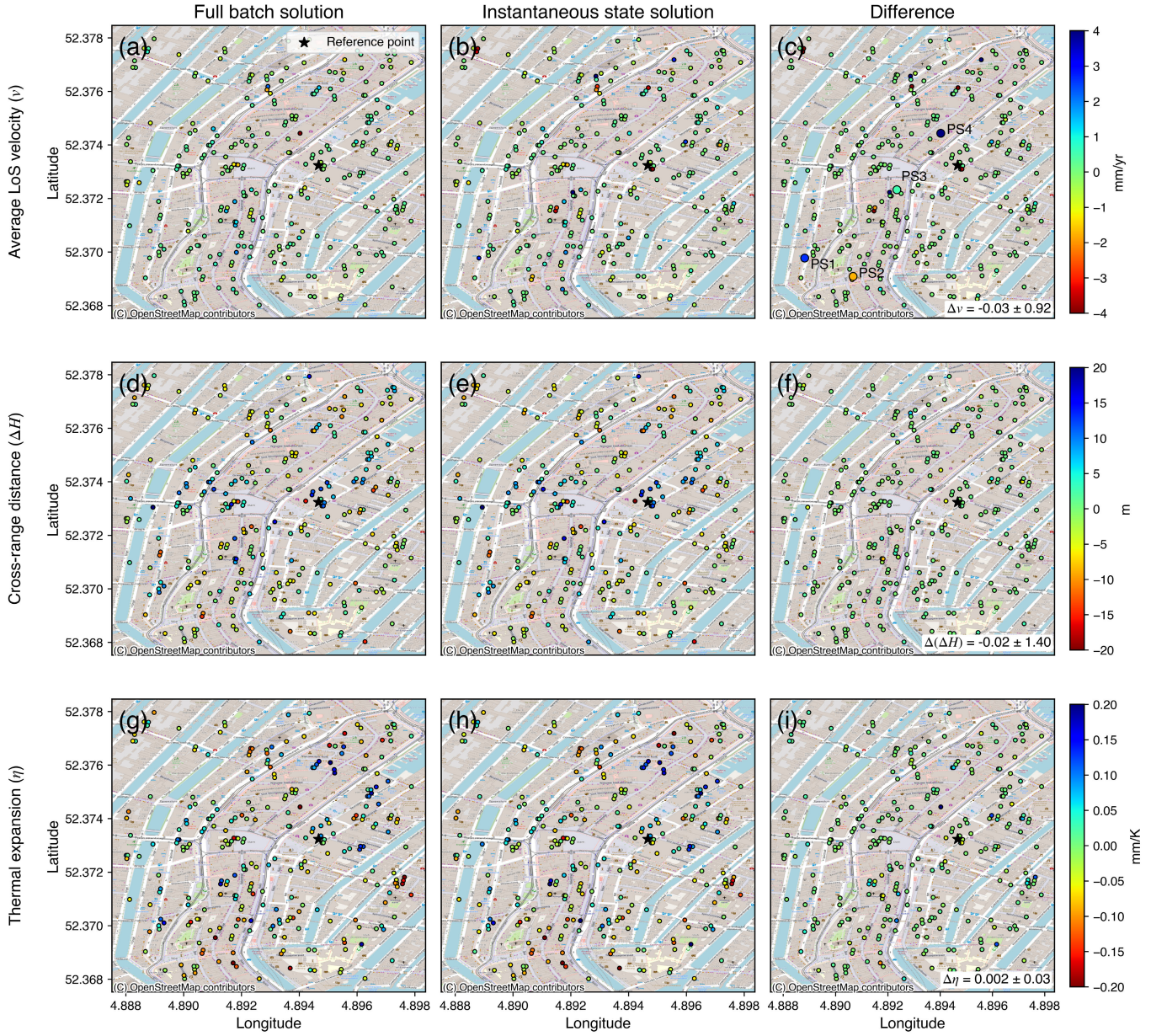

Fig. 8. (a), (d), and (g) Estimated parameters for the full batch solution, (b), (e), and (h) IS solution, and (c), (f), and (i) their difference. The black star represents the reference point, which has the smallest NMAD. (a)–(c) Average LoS velocity v. (d)–(f) Cross-range distance ΔH. (g)–(i) Thermal expansion factor η. The IS solutions for ΔH and η are the estimates from the last epoch of the time series. The predominance of green dots in (c), (f), and (i) indicates that the IS solution on par with the full batch solution. In (c), PS1–PS4 show a relatively large difference in the two solutions. Their displacement time series are shown in Fig. 9.

implicitly, i.e., *during* the estimation of the parameters or states.

It is important to emphasize that the smoothness constraints are not parameters that need to be, should be, or can be estimated from the data. Rather, they are based on prior expectations of the dynamic behavior of the objects in the AoI. As such, the choice for the values of the smoothness constraints is comparable to the choice of estimating a particular parametric model (e.g., "linear plus sinusoidal") in conventional batch estimation. Thus, a misspecification of the smoothness parameters would result in overfitting or underfitting. For this reason, providing realistic but conservative values is recommended. We find that for data with modest quality or better, the sensitivity of the result to the numerical values of the smoothness parameters is limited, i.e., similar estimates result from different combinations of σ_v and τ, see Fig. 10(b) and (c).

V. Discussion

In the following, we compare the proposed method with existing approaches for sequential estimation, analyze smoothness parameter selection, assess the computational efficiency, and discuss the challenges and future perspectives.

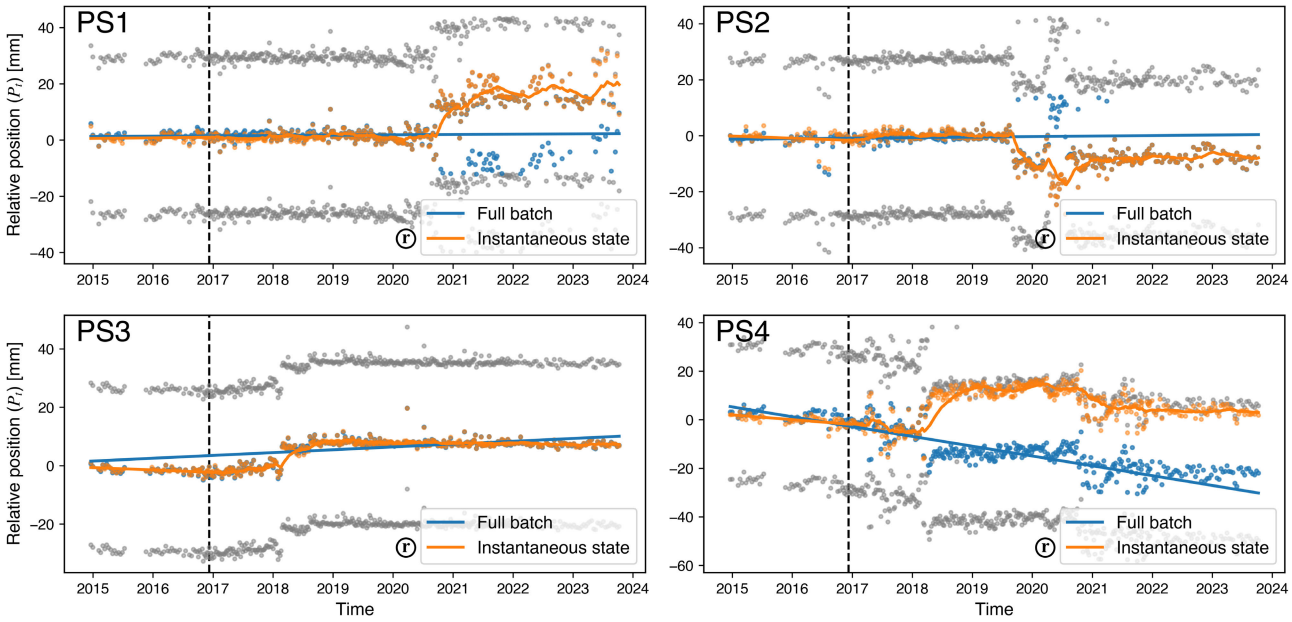

Fig. 9. Estimated relative positions P_t of PS1–PS4 [see Fig. 8(c)] relative to the reference point. The blue line model reflects the hindsight batch constant velocity model, while the orange line represents the instantaneous relative position, only based on retrospective observations, i.e., for each epoch looking back in time. The gray dots indicate the adjacent ambiguity levels, as in Fig. 10. PS1: the quality and behavior of the time series fluctuated since mid-2020. The IS method is able to adjust its estimates accordingly, while the batch method fails to do so, resulting in potential unwrapping errors. PS2: a change in behavior is observed around mid-2019. The IS solution seems to reflect the dynamics of the point more accurately, whereas the batch estimation lacks the flexibility to adapt to the change. PS3: the IS solution seems to be more representative in capturing the actual dynamic behavior of the point. PS4: the two solutions diverge, exhibiting distinct behaviors in early 2018.

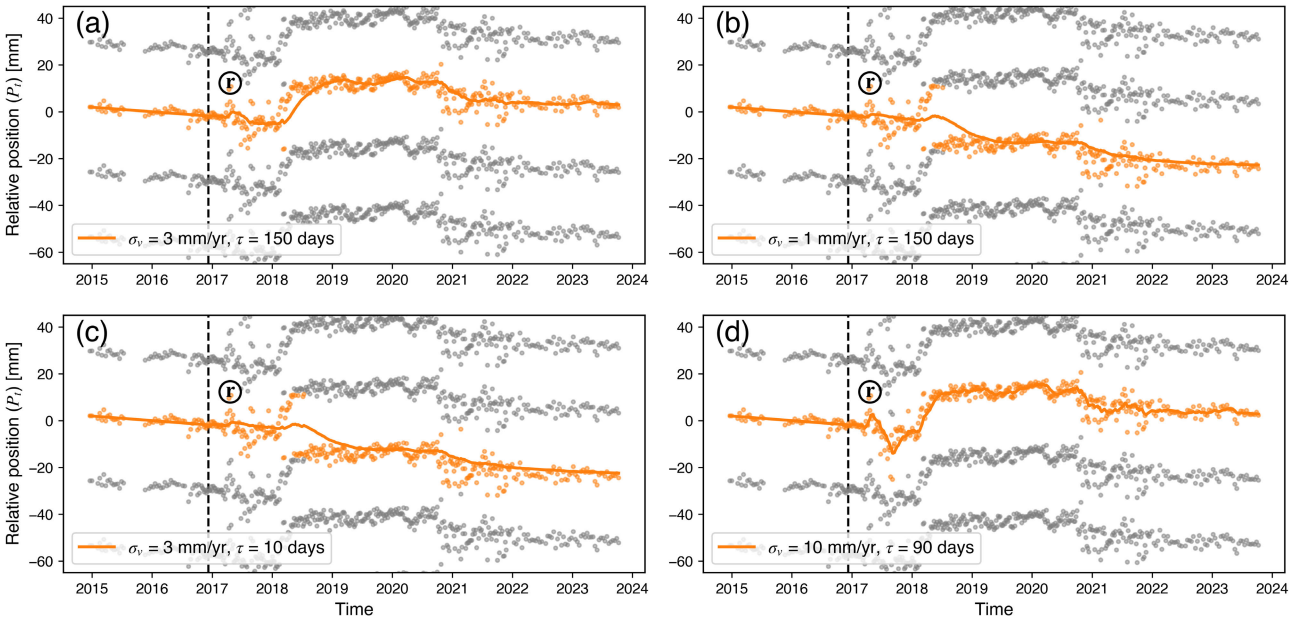

Fig. 10. Influence of the smoothness constraints on the signal for PS4 relative to the reference point shown in Fig. 8(a). The plots show the positions with varying constraints $[\sigma_v, \tau]$, i.e., (a) $[3, 150]$ (default), (b) $[1, 150]$, (c) $[3, 10]$, and (d) $[10, 90]$, in (mm/year) and (days). The different solutions indicate that the choice of the smoothness parameters enables the implicit phase unwrapping.

A. *Comparison of Methods for Sequential Estimation*

Here, we compare the IS method with existing sequential and recursive estimation approaches. In the incremental batch scheme employed, see Fig. 7, parameters are re-estimated upon the arrival of each new observation. Therefore, this procedure is mathematically equivalent to the recursive estimation with a static (constant velocity) model. Existing sequential estimation methods typically rely on time-invariant (static) parameterization. Some approaches directly update the displacement phase estimates, often using interferograms generated between the recent acquisition and earlier ones; consequently, such methods are commonly adopted within SBAS frameworks [11], [12]. Other approaches perform updates by imposing an identical state transition on a certain state component, e.g., a

constant velocity [17], [19]. Still others update the estimates by assuming predefined global deformation models, such as polynomial, sinusoidal, or Heaviside functions [15]. In general, these parameterization strategies are static, as they do not explicitly account for the dynamic evolution of displacement between epochs.

In comparison, the method proposed in this study is a recursive least-squares estimator that is mathematically equivalent to the Kalman filter. This IS method recursively updates the parameters with single new observations by describing the motion of a PS as a function of the position and temporally correlated instantaneous velocity, instead of parameters that describe the behavior of the scatterer over the entire observation period, i.e., in hindsight. The novelty of the exponentially correlated velocity model lies in its physically motivated dynamic formulation. The exponentially correlated (Ornstein–Uhlenbeck) velocity model assumes that velocity evolves with a correlation time τ, leading to a temporally correlated and mean-reverting velocity that constitutes a physically constrained stochastic model for the process noise. By parameterizing the velocity through a standard deviation σ_v and a decorrelation time τ, the model enables direct and interpretable control over both short-term variability and long-term trends, making the imposed smoothness transparent and tunable. Moreover, the resulting mean-reverting dynamics provide a displacement model that better reflects the processes of gradual motion change.

B. Smoothness Parameter Selection

IS InSAR relies on a realistic choice for selecting the values of the smoothness parameters σ_v and τ. This choice is dependent on the particular use case, and the method is therefore not that suitable for *application-agnostic* cases, such as wide-area maps covering multiple deformation phenomena. Instead, the method is more suitable for *application-aware and application-aligned* cases, where a particular dynamic behavior of an object or area can be expected.

Although the selection of smoothness parameters may appear to introduce prior information that is not available beforehand, it is in fact similar to the a priori choice of a specific functional model in conventional InSAR parameter estimation. Such choices likewise rely on prior expectations about the dynamic behavior of the object or area under study. For example, the archetypal constant-velocity model may be interpreted as implying effectively "infinite smoothness," i.e., $\sigma_v < 0.1$ mm/year and $\tau > 365$ days; whether such assumptions are realistic is left to the reader.

We emphasize that inferring the parameters directly from the data would be conceptually incorrect, since the smoothness criteria are related to the underlying signal and not to the observations.

C. Computational Efficiency

For the *IS estimation approach*, the computational effort for each updated epoch is independent of the length of the time series up to that epoch, since the solution at each epoch is obtained directly from the previous one, requiring only a single update step. Both the *incremental batch* and *full batch* approaches exhibit computational costs that grow rapidly with the number of epochs. This stems from the need to repeatedly solve a system of equations involving all available epochs whenever a new observation is introduced. As the number of epochs increases, the resulting computational burden escalates significantly. From a monitoring perspective in an urban setting, with millions of PSs requiring updates whenever a new acquisition becomes available, this results in a substantial increase in computational cost. In contrast, the IS estimation approach remains scalable in terms of memory, as it does not require storing long temporal historical data. Since it is designed for near real-time monitoring, the processing is carried out at each epoch instead of only once covering the full time series. As a result, computational demands grow linearly with the number of arcs, and the epoch-wise implementation allows for straightforward parallelization.

D. Challenges and Perspectives

Although the IS estimation method incorporates the smoothness constraints explicitly, discontinuities in displacement or anomalous observations can still affect the estimation. As an example, in Fig. 10, a displacement discontinuity occurred in early 2018. Whether or not it is possible to detect displacement discontinuities and outliers depends on the choice of the numerical values of the smoothness parameters τ and σ_v. When the underlying assumption is that displacement evolves smoothly in time, displacement discontinuities that violate this assumption will be smoothened out, see Fig. 10(b) and (c), leading to biased estimates in the epochs right after the discontinuities. However, because the IS estimation method processes observations sequentially and updates the position and velocity at each epoch, the filter can recover after the discontinuity as subsequent observations gradually reduce the influence of the prior states. In such a case, one may examine the predicted residuals at the corresponding epochs to identify potential displacement anomalies that warrant further investigation. Alternatively, if such discontinuities are expected to occur, the smoothness parameters can be chosen to allow the model to adapt to them.

On the other hand, outliers can also introduce undesirable updates in the state estimation when processed as single observations. In practice, this issue can be mitigated by incorporating outlier detection tests on the predicted residual between the prediction and the observation at the corresponding epochs.

While displacement discontinuities and outliers can influence the estimates, the proposed dynamic formulation can accommodate their effects to some extent. We consider the explicit handling of such cases as an important direction for future work.

Furthermore, the proposed framework for IS estimation is applied to a limited AoI within the built environment, see Fig. 8. In future work, the framework will be extended to multiple real-world applications to further evaluate its feasibility, robustness, and practical applicability across diverse scenarios.

VI. Conclusion

We present a novel framework to parameterize, predict, and analyze the motion of InSAR scatterers. It uses an IS vector,

which is explicitly time-indexed and governed by a dynamic model. The estimation and prediction of the state vector are recursive and causal. We introduce contextual smoothness constraints on the displacement signal by modeling the instantaneous velocity as an exponentially correlated, mean-reverting Ornstein–Uhlenbeck process. *IS InSAR* is explicitly designed around a defining yet underexploited feature of satellite InSAR: the systematic and frequent updating of time series with each new acquisition. It is more flexible than the conventional time-invariant global parameterization, which is typically applied uniformly to all scatterers within the AoI and does not readily adapt to changes in a scatterer's dynamic behavior. Moreover, it enables the assessment of the likelihood of alternative ambiguity solutions. Finally, it is computationally more efficient, as new acquisitions do not require re-evaluating past observations, enabling near real-time monitoring.

External contextual information on the expected variability of the displacement signal is required to choose smoothness constraints that are appropriate for a particular use case. The impact of this selection is evaluated for particular cases in this study; however, there is still a need for experiments on broader range of scenarios. Future work will focus on the development of testing procedures for IS InSAR.

Appendix

In Section III-A, temporal correlation is introduced as a smoothness constraint in the state transitions. This constraint is inferred on $\Phi_{t,t-1}$ and d_t in the *time update*, see (14). In the following, we: 1) elaborate on the rationale for employing an exponentially correlated velocity model in the state transition and 2) derive the variance–covariance matrix Q_{d_t}. Our approach is based on the assumption that the velocity at a given time is statistically related to its past values, and this dependence decays exponentially with increasing time difference, using an exponentially correlated zero-mean velocity model proposed by Teunissen [20].

An exponentially correlated random function can be characterized as the solution to a first-order stochastic differential equation driven by white noise, i.e., an Ornstein–Uhlenbeck process [21] to describe velocity. This means the velocity has memory (temporal correlation), but this memory fades exponentially, and over time the process tends to drift toward its mean function, i.e., it is *mean reverting*. Consequently, we define the zero-mean velocity v_t by the differential equation [20]

$$\dot{v}_t = -\rho v_t + z(\zeta) \tag{26}$$

with

$$\begin{aligned} \sigma_{zz}(\zeta) &= 2\rho\sigma_v^2\delta(\zeta) \ \text{(white noise)} \\ \sigma_{v_{t_0}^2} &= \sigma_v^2 \\ \sigma_{(Dv)_{t_0}} &= 0,\ \sigma_{(vz)_{t_0}} = 0 \quad \forall t \\ E\left\{\underline{v}_{t_0}\right\} &= 0,\ E\left\{\underline{v}_t\right\} = 0 \quad \forall t \end{aligned} \tag{27}$$

where $z(\zeta)$ is a white noise random function, $\rho > 0$ is the correlation decay rate or damping function (greater ρ = faster decay), $\delta(\zeta)$ is the Dirac delta function, and $\int_{-\infty}^{\infty}\delta(\zeta)d\zeta = 1$. We use the decorrelation time $\tau = 1/\rho$ (i.e., greater decorrelation time = slower decay) in this study.

Following (26), the IS x_t, see (11), can be described by the following differential equation:

$$\underbrace{\begin{bmatrix} \dot{D}_t \\ \dot{v}_t \\ \Delta\dot{H}_t \\ \dot{\eta}_t \end{bmatrix}}_{\dot{\underline{x}}_t} = \underbrace{\begin{bmatrix} 0 & 1 & 0 & 0 \\ 0 & -\rho & 0 & 0 \\ 0 & 0 & 0 & 0 \\ 0 & 0 & 0 & 0 \end{bmatrix}}_{F} \underbrace{\begin{bmatrix} D_t \\ v_t \\ \Delta H_t \\ \eta_t \end{bmatrix}}_{\underline{x}_t} + \underbrace{\begin{bmatrix} 0 \\ 1 \\ 0 \\ 0 \end{bmatrix}}_{G} z_t. \tag{28}$$

Its unique solution is given by [20]

$$x_t = e^{F\Delta t}x_{t_0} + \int_{\zeta=t_0}^{t} e^{F(t-\zeta)}\,G\,z(\zeta)\,d\zeta \tag{29}$$

where $\Delta t = t - t_0$. The epoch t_0 can be adjusted to epoch $t-1$ in the context of the recursive update, i.e.,

$$x_t = e^{F\Delta t}x_{t-1} + \int_{\zeta=t-1}^{t} e^{F(t-\zeta)}\,G\,z(\zeta)\,d\zeta \tag{30}$$

where Δt indicates the absolute time difference between epoch t and $t-1$. This solution is equivalent to the *time-update equation*, see (14), and the transition matrix $\Phi_{t,t-1}$, see (16), corresponds with $e^{F\Delta t}$, i.e.,

$$\Phi_{t,t-1} = e^{F\Delta t} = \begin{bmatrix} 1 & \tau\left(1 - e^{-\frac{\Delta t}{\tau}}\right) & 0 & 0 \\ 0 & e^{-\frac{\Delta t}{\tau}} & 0 & 0 \\ 0 & 0 & 1 & 0 \\ 0 & 0 & 0 & 1 \end{bmatrix}. \tag{31}$$

With (27) and (30), the stochasticity of d_t expressed by Q_{d_t}, see (17), is given by [20]

$$\begin{aligned} Q_{d_t} &= \int_{\zeta=t-1}^{t} \frac{2\sigma_v^2}{\tau}\left(e^{F(t-\zeta)}\right)^{\top} G^{\top} G\, e^{F(t-\zeta)} d\zeta \\ &= \sigma_v^2 \begin{bmatrix} q_{11} & & & sym. \\ q_{21} & q_{22} & & \\ 0 & 0 & 0 & \\ 0 & 0 & 0 & 0 \end{bmatrix} \end{aligned} \tag{32}$$

elaborated further in (17).

Data Availability

A simulation tool is provided that allows adjustment ofthe velocity standard deviation σ_v and velocity decorrelation time τ, enabling the generation of noise-free simulated signals for selecting appropriate parameter settings, see https://github.com/TUDelftGeodesy/Smoothness-constraints-for-instantaneous-state-InSAR

Acknowledgment

The authors would like to thank European Space Agency (ESA) for the free provision of Sentinel-1 data, and also would like to thank the reviewers and editors for their valuable comments.

References

[1] R. F. Hanssen, *Radar Interferometry: Data Interpretation and Error Analysis*. Kluwer Academic, The Netherlands: Kluwer Academic, 2001.

[2] L. Chang, R. P. B. J. Dollevoet, and R. F. Hanssen, "Nationwide railway monitoring using satellite SAR interferometry," *IEEE J. Sel. Topics Appl. Earth Observ. Remote Sens.*, vol. 10, no. 2, pp. 596–604, Feb. 2017.

[3] A. Ferretti, C. Prati, and F. Rocca, "Permanent scatterers in SAR interferometry," *IEEE Trans. Geosci. Remote Sens.*, vol. 39, no. 1, pp. 8–20, Jan. 2001.

[4] F. J. van Leijen and R. F. Hanssen, "Persistent scatterer density improvement using adaptive deformation models," in *Proc. IEEE Int. Geosci. Remote Sens. Symp.*, May 2007, pp. 2102–2105.

[5] F. J. van Leijen, "Persistent scatterer interferometry based on geodetic estimation theory," Ph.D. dissertation, Dept. Geosci. Remote Sens., Delft Univ. Technol., Delft, The Netherlands, 2014.

[6] L. Chang and R. F. Hanssen, "A probabilistic approach for InSAR time-series postprocessing," *IEEE Trans. Geosci. Remote Sens.*, vol. 54, no. 1, pp. 421–430, Jan. 2016.

[7] Q. Verburg, "QUInSAR: Temporal parameter and ambiguity estimation using recursive least-squares: A methodology for persistent scatterer interferometry," M.S. thesis, Dept. Geosci. Remote Sens., Delft Univ. Technol., Delft, The Netherlands, 2017.

[8] Y. Wang, W. S. Brouwer, F. J. van Leijen, and R. F. Hanssen, "Constrained recursive parameter estimation for InSAR Arcs," in *Proc. IEEE Int. Geosci. Remote Sens. Symp.*, Sep. 2024, pp. 10689–10693.

[9] R. E. Kalman, "A new approach to linear filtering and prediction problems," *Trans. ASME-J. Basic Eng.*, vol. 82, no. 1, pp. 35–45, Mar. 1960.

[10] H. Ansari, F. De Zan, and R. Bamler, "Sequential estimator: Toward efficient InSAR time series analysis," *IEEE Trans. Geosci. Remote Sens.*, vol. 55, no. 10, pp. 5637–5652, Oct. 2017.

[11] J. Xu, M. Jiang, V. G. Ferreira, and Z. Wu, "Time-series InSAR dynamic analysis with robust sequential adjustment," *IEEE Geosci. Remote Sens. Lett.*, vol. 19, pp. 1–5, 2022.

[12] B. Wang, Q. Zhang, C. Zhao, A. Pepe, and Y. Niu, "Near real-time InSAR deformation time series estimation with modified Kalman filter and sequential least squares," *IEEE J. Sel. Topics Appl. Earth Observ. Remote Sens.*, vol. 15, pp. 2437–2448, 2022.

[13] B. Wang, C. Zhao, Q. Zhang, Z. Lu, Z. Li, and Y. Liu, "Sequential estimation of dynamic deformation parameters for SBAS-InSAR," *IEEE Geosci. Remote Sens. Lett.*, vol. 17, no. 6, pp. 1017–1021, Jun. 2020.

[14] J. Liu et al., "Dynamically estimating deformations with wrapped InSAR based on sequential adjustment," *J. Geodesy*, vol. 97, no. 5, pp. 1–20, May 2023.

[15] M. Dalaison and R. Jolivet, "A Kalman filter time series analysis method for InSAR," *J. Geophys. Research: Solid Earth*, vol. 125, no. 7, pp. 1–21, Jul. 2020.

[16] P. S. Marinkovic, F. van Leijen, G. Ketelaar, and R. F. Hanssen, "Recursive data processing and data volume minimization for PS-InSAR," in *Proc. IEEE Int. Geosci. Remote Sens. Symp.*, vol. 4, Aug. 2005, pp. 2697–2700.

[17] F. Hu, F. J. van Leijen, L. Chang, J. Wu, and R. F. Hanssen, "Combined detection of surface changes and deformation anomalies using amplitude-augmented recursive InSAR time series," *IEEE Trans. Geosci. Remote Sens.*, vol. 60, 2022, Art. no. 5210816.

[18] J. Cai et al., "A new algorithm for landslide dynamic monitoring with high temporal resolution by Kalman filter integration of multiplatform time-series InSAR processing," *Int. J. Appl. Earth Observ. Geoinformation*, vol. 110, Jun. 2022, Art. no. 102812.

[19] Y. Liu, C. Xu, and Y. Wen, "Adaptive robust Kalman filter-based InSAR time series analysis for deformation monitoring," *Adv. Space Res.*, vol. 77, no. 4, pp. 4168–4183, Feb. 2026.

[20] P. J. G. Teunissen, *Dynamic Data Processing: Recursive Least-Squares*, 2nd ed., Delft, The Netherlands: TU Delft Open Publishing, 2024.

[21] G. E. Uhlenbeck and L. S. Ornstein, "On the theory of the Brownian motion," *Phys. Rev.*, vol. 36, pp. 823–841, Sep. 1930.

[22] A. Ferretti, A. Fumagalli, F. Novali, C. Prati, F. Rocca, and A. Rucci, "A new algorithm for processing interferometric data-stacks: SqueeSAR," *IEEE Trans. Geosci. Remote Sens.*, vol. 49, no. 9, pp. 3460–3470, Sep. 2011.

[23] F. Hu, J. Wu, L. Chang, and R. F. Hanssen, "Incorporating temporary coherent scatterers in multi-temporal InSAR using adaptive temporal subsets," *IEEE Trans. Geosci. Remote Sens.*, vol. 57, no. 10, pp. 7658–7670, Oct. 2019.

[24] P. Conroy, S. A. N. van Diepen, F. J. van Leijen, and R. F. Hanssen, "Bridging loss-of-lock in InSAR time series of distributed scatterers," *IEEE Trans. Geosci. Remote Sens.*, vol. 61, 2023, Art. no. 5220911.

[25] P. J. G. Teunissen, "Least-squares estimation of the integer GPS ambiguities," in *Proc. Invited Lect., Sect. IV Theory Methodol. Int. Assoc. Geodesy (IAG) Gen. Meeting*. Beijing, China: Delft Geodetic Computing Centre, Aug. 1993.

[26] B. M. Kampes and R. F. Hanssen, "Ambiguity resolution for permanent scatterer interferometry," *IEEE Trans. Geosci. Remote Sens.*, vol. 42, no. 11, pp. 2446–2453, Nov. 2004.

[27] P. J. G. Teunissen, "The least-squares ambiguity decorrelation adjustment: A method for fast GPS integer ambiguity estimation," *J. Geodesy*, vol. 70, nos. 1–2, pp. 65–82, Nov. 1995.

[28] H. Fattahi and F. Amelung, "DEM error correction in InSAR time series," *IEEE Trans. Geosci. Remote Sens.*, vol. 51, no. 7, pp. 4249–4259, Jul. 2013.

[29] W. S. Brouwer, Y. Wang, F. J. van Leijen, and R. F. Hanssen, "On the stochastic model for InSAR single arc point scatterer time series," in *Proc. IEEE Int. Geosci. Remote Sens. Symp. (IGARSS)*, Jul. 2023, pp. 7902–7905.

[30] W. S. Brouwer and R. F. Hanssen, "On the definition of an independent stochastic model for InSAR time series," *IEEE Trans. Geosci. Remote Sens.*, vol. 63, 2025, Art. no. 4508311.

[31] C. Truong, L. Oudre, and N. Vayatis, "Selective review of offline change point detection methods," *Signal Process.*, vol. 167, Feb. 2020, Art. no. 107299.

[32] G. Strang, *Introduction to Linear Algebra*, 5th ed., Reading, MA, USA: Addison-Wesley, 2016.

[33] A. V. Oppenheim and G. C. Verghese, *Signals, Systems and Inference*. London, U.K.: Pearson, 2017.

[34] Y. Wang, W. S. Brouwer, F. J. Van Leijen, and R. F. Hanssen, "Non-parametric InSAR time series analysis of arcs using complex B-splines," in *Proc. IEEE Int. Geosci. Remote Sens. Symp.*, Jul. 2023, pp. 8238–8241.

Yuqing Wang received the M.Sc. degree in geophysics from Sun Yat-sen University, Zhuhai, China, in 2021. She is currently pursuing the Ph.D. degree with Delft University of Technology, Delft, The Netherlands.

Her research interests include time series analysis, near real-time deformation monitoring and change detection using satellite radar interferometry.

Wietske S. Brouwer received the B.Sc. and M.Sc. degrees in civil engineering from Delft University of Technology, Delft, The Netherlands, in 2018 and 2021, respectively, where she is currently pursuing the Ph.D. degree, working on mathematical aspects of satellite radar interferometry.

Freek J. van Leijen (Member, IEEE) received the master's degree in geodetic engineering from Delft University of Technology, Delft, The Netherlands, in 2002, and the Ph.D. degree from Delft University of Technology in 2014, with a focus on InSAR research. His thesis concerned the stochastic modeling of the tropospheric variability using GPS and InSAR observations.

He has developed a range of software algorithms for persistent scatterer interferometry. After working for five years at SkyGeo, Delft, a commercial company delivering radar remote-sensing services, he returned to Delft University of Technology in 2013 to continue his research in the field of satellite radar interferometry.

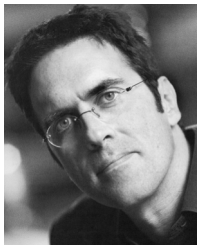

Ramon F. Hanssen (Senior Member, IEEE) received the M.Sc. degree in geodetic engineering and the Ph.D. degree (cum laude) from Delft University of Technology, Delft, The Netherlands, in 1993 and 2001, respectively.

He was with the International Institute for Aerospace Survey and Earth Science (ITC), Stuttgart University, Stuttgart, Germany; German Aerospace Center (DLR), Weßling, Germany; Stanford University, Stanford, CA, USA, as a Fulbright Fellow; and the Scripps Institution of Oceanography, University of California, San Diego, La Jolla, CA, USA, involved in microwave remote sensing, radar interferometry, signal processing, and geophysical application development. Since 2008, he has been an Antoni van Leeuwenhoek Professor in Earth observation with Delft University of Technology, where he has been leading the research group on mathematical geodesy and positioning since 2009. He has authored a textbook on radar interferometry.